Initial Development of a Quadcopter Simulation Environment for Auralization

Andrew Christian
Research Engineer (Psychoacoustics)
Structural Acoustics Branch
NASA Langley Research Center
Hampton, VA, U.S.A.

Joseph Lawrence
Undergraduate (Physics)
College of Physical and Mathematical Sciences
Brigham Young University
Provo, UT, U.S.A.

ABSTRACT

This paper describes a recently created computer simulation of quadcopter flight dynamics for the NASA DELIVER project. The goal of this effort is to produce a simulation that includes a number of physical effects that are not usually found in other dynamics simulations (e.g., those used for flight controller development). These effects will be shown to have a significant impact on the fidelity of auralizations — entirely synthetic time-domain predictions of sound — based on this simulation when compared to a recording. High-fidelity auralizations are an important precursor to human subject tests that seek to understand the impact of vehicle configurations on noise and annoyance.

INTRODUCTION

Given the continuing proliferation of small unmanned aerial systems (sUAS) of all sizes and flight capabilities, as well as the innumerable concepts that entrepreneurs around the world have thought of for their use, it is only a matter of time before communities will be faced with large swarms of these machines in close proximity to humans. This situation will likely create many problems: safety, privacy, etc. One of the principal issues may become noise and annoyance.

At NASA, the DELIVER project seeks to get ahead of this problem by working to create a design environment for these novel vertical-lift vehicles. One of the components of this environment will seek to predict the acoustic impact of sUAS systems, evaluated in terms of human annoyance. In order to create such a design tool, researches at NASA will have to create ways to predict not only the acoustic output of these vehicles, but also how that output (which may vary significantly in overall level as well as qualitatively between vehicles) is correlated with human annoyance.

In pursuit of this goal, a computer simulation of a quadcopter was developed that takes into account several aeromechanical effects that are not typically implemented in sUAS simulations. This simulation can be combined with an existing capability to generate auralizations — completely synthetic sounds based on the simulation outputs (this process is detailed in many previous publications, the most pertinent being by Christian (Ref. 1), and Rizzi (Ref. 2)). These auralizations can then be evaluated by human subjects in a controlled environment such as the Exterior Effects Room at NASA Langley Research Center (Refs. 3, 4), in order to explore the relationship between the input parameters of the simulation (e.g., quadcopter design parameters, control parameters, etc.) and the human annoyance generated by the resulting sounds.

Throughout this paper, spectrograms based on auralizations and a recording of quadcopters will be presented. The reader is encouraged to access the openly available wave-file versions of these sounds and "listen along" as they are discussed in this paper. The sounds can be found on the NASA Structural Acoustics website:

http://stabserv.larc.nasa.gov/flyover/

Operational Concepts

For smaller quadcopters, like the DJI Phantom II that will be used in this study, the speeds of the four rotors (measured in revolutions-per-minute (rpm)) are controlled directly through variable speed motors. A simple proportional/integral/derivative (PID) closed-loop feedback control system on the vehicle modulates the speed of the individual rotors in order to maintain the vehicle's attitude. For instance, in the case of forward flight, the speed of the two stern motors are increased, while the the bow motors are kept near hover speed. This causes the vehicle to pitch forward. The PID system maintains the overall lift of the vehicle in order to resist gravity, and the component of the total force generated by the rotors that is not pointed directly skyward causes a net thrust force to act on the vehicle generating motion in that direction. This approach leads to constantly-changing and unequal rotor speeds that in turn leads to perceptually significant frequency modulation of the rotor noise.

The Phantom II was among an array of vehicles included in a recent series of outdoor vehicle flight tests conducted by NASA (Ref. 5). The purpose of these flight tests was to acquire acoustic and flight telemetry data for the vehicle while operating under realistic flight conditions. Some sam-

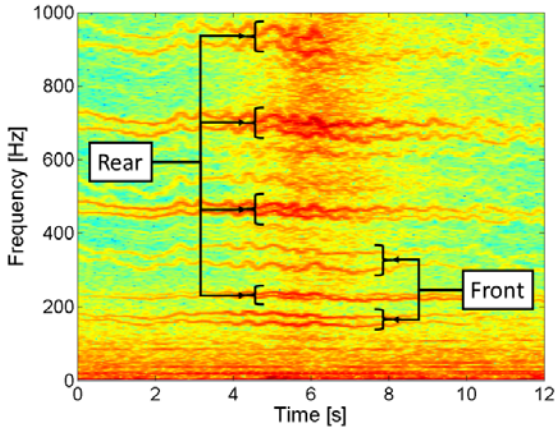

Fig. 1. Spectrogram of recorded quadcopter flyover.

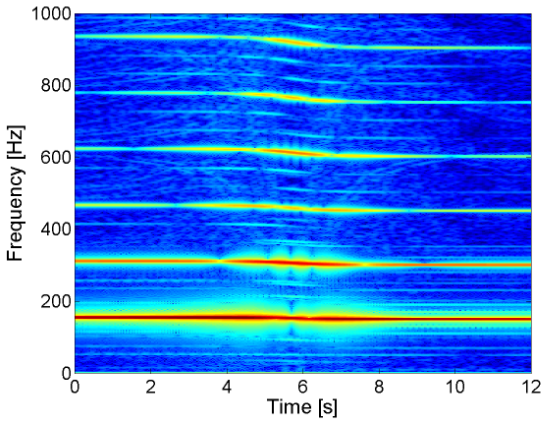

Fig. 2. Spectrogram of auralization of basic simulation output.

ple acoustic data from a nominally straight and level overhead flight of the Phantom 2 is provided in Figure 1. The pairs of lines running relatively horizontally through the figure represent blade passage frequency (BPF) harmonics of the front and rear pairs of rotors. Momentary variation within pairs indicates roll compensation, and momentary variation between the pairs indicates pitch compensation. These sorts of variations are clearly audible as the vehicle control system constantly makes adjustments in order maintain forward flight in the presence of wind, turbulence, and mass loading by the payload. It is likely that the annoyance caused by sUAS will have some component that is correlated with the attributes of these variations (for example, see recent work by Palumbo (Ref. 6)). The ability to accurately simulate and auralize these features of the noise would allow for the controlled human subject testing needed to evaluate how these modulations, as well as other factors, contribute to the annoyance generated by these machines.

Extant Simulators

Most contemporary quadcopter simulations only include the basic mechanics of quadcopter flight. For most applications, these simulations are run in order to test and develop control schemes for sUAS. The concept behind taking such a simple approach to modeling is that if a control system can be shown to be robust enough to control a vehicle under these basic conditions, the addition of smaller effects such as slight atmospheric turbulence should not affect the controllers overall ability to keep the vehicle aloft. Further, many of these effects can be computationally expensive so that it is easy to deem their inclusion in simulations unnecessary if they are not likely to greatly impact the outcome.

As an example, consider the spectrogram of Figure 2.[1] This shows an auralization that was based on the output of a quadcopter dynamics model named Quad-Sim (see Hartman (Ref. 7), discussed further below). In this case, there is no drag or turbulence. This means that once the quadcopter gets up to speed (an event that takes place before time = 0 s in Fig. 2), the vehicle can right itself and cut horizontally though the air — effectively hovering while sliding in the intended direction. This is patently unrealistic and there are multiple physical effects that, in the real world, perturb and resist this flight operation. Some of these effects have been pointed out in the past by sUAS researches (e.g., see Mahony (Ref. 8) and Bangura (Ref. 9)).

There are many clear audible differences between the sounds represented in Figs. 1 and 2. Perhaps the primary deficiency is that the BPFs of all four rotors are perfectly the same for the entire time shown. This shortcoming, as well as others are addressed implicitly by the addition of the aeromechanical effects discussed below that are left out of the Quad-Sim model.

The rest of this document is divided into two main parts. The first two following sections detail the source of the simulator created for this effort. First, the basis of the simulation is described as a port of a commonly available program. Second, the added aeromechanical effects are described along with the various assumptions and approximations needed to interface those effects with the existing simulation.

The Auralization Results section shows a series of spectrograms (similar to that shown in Fig. 2) which incrementally add the aeromechanical effects. The impact of these addi-

[1]For all of the spectrograms shown here, the processing settings (the frequency and time steps) have been matched closely between the various source materials. The simulations shown are all based on the attributes of the flyover from Fig. 1. Also, the color scale of each is normalized to the peak of that figure, although the dynamic range of the color scale is the same between all spectrograms (e.g., the 'background' of Fig. 1 is not as dark of a blue as that of Fig. 2 as there is ambient noise on the recording whereas the auralization contains only the BPFs and their harmonics). Color figures available online.

tions on the resulting auralizations are discussed along with the likely importance of the inclusion of these effect on the perception of the sound of the quadcopter.

THE DYNAMICS MODEL

This section introduces the sources of the core dynamics model used for the simulation. For the sake of brevity, no equations are given in this section, as the references upon which this work is based are freely available and extensively documented.

Quad-Sim

The core dynamics of this simulation are derived from Quad-Sim, an open source quadcopter model implemented in MATLAB Simulink (see Hartman (Ref. 7)). Earlier work by Mahony (Ref. 8) is the basis for many of the equations used in Quad-Sim.

The starting point for this effort was to use the dynamics model of a quadcopter in the 'x' configuration — the case where the direction of flight is between two rotors so that there are two front rotors and two rear rotors as discussed above[2]. This model provides the formulations for the mass moment of inertia matrix based on the physical properties (i.e., mass distribution) of the vehicle under study, the gyroscopic moments that affect the vehicle, and the state equation formulation for the vehicle. Although Quad-Sim does not include aerodynamic effects, places to add them are available. Quad-Sim was also used as the basis for the model of the on-board PID controller.

Procedural Port

The freely available version of Quad-Sim is programmed in MATLAB Simulink, which is a graphical environment. One of the first steps in this effort was to port Quad-Sim to completely procedural MATLAB without the use of functions belonging to 'toolboxes.' This was done both to gain more control over the simulation and to facilitate possible future translations to other procedural languages, such as C, that can interface more easily with the auralization tools currently in use at NASA (i.e., the NASA Auralization Framework, see Aumann (Ref. 10)).

In order to create this port, an order-4 Runge-Kutta (an explicit forward-time stepping) ODE solver was created to operate on the state equations of the Quad-Sim model (see, for example, Atkinson and Han (Ref. 11)). A time step of .001 s was found to give results that were convergent in all tested cases and generated rpm time histories with an error of less than 1 rpm — suitably accurate for this effort.

[2]The Quad-Sim model also has provisions for a '+' configuration in which there is one front rotor, one rear rotor, and two rotors which flank the center of mass. This capability was disregarded for this effort as the DJI Phantom II runs only in an 'x' configuration.

The original Quad-Sim implementation was then used to benchmark the port. It was found that not only was the port more accurate than the original (in terms of error in rpm), but also, for the non-extended model, that it ran more quickly than Quad-Sim.

MODEL EXTENSIONS

This section discusses extensions that were added to the basic dynamics model. The only equations and methods that will be given here are those that do not appear comprehensively in any single source. For instance, equations are given when intermediate steps and approximations are necessary in order to interface the core model with either the model extensions or the input data available. Otherwise readers are encouraged to look to the references for the complete background and technical details of the different extensions.

Rotorcraft Aeromechanics

The first and most fundamental change that was made to the model was to upgrade the aeromechanics that were included in the original Quad-Sim program. The new model follows the development of work by Hoffman (Ref. 12), and uses fundamentals from textbooks by Prouty (Ref. 13) and Leishman (Ref. 14). The results used here come from actuator disc theory.

Rotor Coefficients:

The original Quad-Sim model requires separate specification of 3 lumped parameter coefficients that define the performance of the rotor/motor combination. These are the thrust, torque, and power coefficients, the standard non-dimensional versions of which are:

$$C_T = \frac{T}{\rho A \omega^2 R^2} \tag{1}$$

$$C_Q = \frac{Q}{\rho A \omega^2 R^3} \tag{2}$$

$$C_P = \frac{P}{\rho A \omega^3 R^3} \tag{3}$$

In Equations 1-3, ρ is the density of the air, A is the cross-sectional area of the rotor's rotation, ω is the angular velocity of the rotor, and R is the radius of the rotor. Using SI units, this gives thrust T in units of Newtons, torque Q in N·m, and power P in $\frac{N \cdot m}{s}$ (Watts).

One of the other activities of the DELIVER project is to measure the acoustic output of rotors and motors isolated from sUAS vehicles while at the same time analyzing their performance characteristics (see Zawodny (Ref. 15)). These measurements produce estimates for the thrust coefficient, but not for the other two. In order to use this information in the simulation, an approximation is made which allows C_P and C_Q to be calculated from the measured C_T.

First, a basic relationship between power and thrust is established using the induced velocity through the rotor while hovering (v_h).

$$P = Tv_h \tag{4}$$

$$v_h = \sqrt{\frac{T}{2\rho A}} \tag{5}$$

These equations simplify to a relationship between C_T and C_P:

$$C_P = \frac{C_T^{3/2}}{\sqrt{2}} \tag{6}$$

This is only strictly valid in the hover condition, though it is used as a constant in this simulation. Another assumption is that power is directly related to torque as $P = \omega Q$. This implies that simply:

$$C_Q = C_P \tag{7}$$

Thus, the 3 coefficients can be fully determined from available experimental data.

Upgraded Aeromechanics:

In the Quad-Sim program, thrust is simply proportional to rotor speed squared. However, more accurately, the quadcopter speed and angle of attack relative to the airflow will change the induced velocity of air through the rotor disk, thus changing the thrust. Thrust can be expressed as the ratio of power to the airflow through the rotor disk:

$$T = \frac{P}{v_\bullet \sin\alpha + v_i} \tag{8}$$

where v_i is the induced velocity, $v_\bullet$ is the magnitude of the air-stream velocity relative to the rotor, and α is the angle of attack (where a positive angle corresponds with pitching forward)[3]. Note that this equation supersedes Eq. 1. In order to calculate the thrust, both v_i and P need to be calculated. Using an expression from Leishman (pp. 64), the induced velocity can be written as:

$$v_i = \frac{v_h^2}{\sqrt{(v_\bullet \cos\alpha)^2 + (v_\bullet \sin\alpha + v_i)^2}} \tag{9}$$

At hover or during a climb, the rotor is in the 'normal working state,' where there is a defined flow of air downward through the rotor and the resultant thrust pushes the rotor upwards. At fast descent velocities, the rotor is in the 'windmill brake state,' where there is a defined flow of air upward through the rotor creating a thrust that pushes the rotor further downwards. Both of these states have simple solutions for the induced velocity given the above equation.

At slow descent velocities, the rotor is in the 'vortex ring state.' This means that air flows downward through the rotor, and then circles back in a toroidal ring around the rotor to before being ingested by the rotor again. In some cases this can cause a turbulent descent condition and even a loss of thrust. However, it is not straightforward to account for the vortex ring state using Equation 9. In most cases, assuming a normal working state for the vortex ring state results in an acceptable approximation that works for all directions of motion, not just climb and descent.[4]

Equation 9 is a transcendental function as v_i appears on both sides. Therefore an indirect method must be used to calculate the current value of v_i. Newton's method is used here to find the solution, though an appropriate initial guess is necessary to make the method converge to the desired solution. In the normal working and vortex ring states, defined as the regime in which the ratio of the apparent vertical velocity W to the induced hover velocity v_h is greater than -2, the guess is:

$$v_{i;0} = -\frac{W}{2} + \sqrt{\frac{V_\bullet}{2} + v_h^2} \tag{10}$$

In the case of the windmill brake state (when $\frac{W}{v_h} < -2$) the guess is:

$$v_{i;0} = -\frac{W}{2} - \sqrt{\frac{V_\bullet}{2} - v_h^2} \tag{11}$$

The Ground Effect:

Finally, there is a modification for the ground effect. When a rotor is close to the ground, the induced air stream is reflected by the ground creating an increase in thrust. The calculation for the ratio of thrust with ground effect compared to the thrust expected in free space comes from Bangura (Ref. 9).

$$\frac{T_{Ground}}{T} = \frac{1}{1 - \left(\frac{r}{4z}\right)^2 \left(1 + \frac{V_\bullet^2}{v_i^2}\right)^{-1}} \tag{12}$$

where z is the height above the ground surface and r is the radius of the whole rotor area. For the quadcopter configuration here this radius is defined as the distance from the quadcopter (hub) center to the rotor center plus the radius of a rotor. This has a negligible effect unless the quadcopter is only a few feet above the ground.

Wind Effects

Before adding effects such as drag, it is necessary to define the air through which the model quadcopter will be moving.

[3]Both $v_\bullet$ and α can be calculated from the apparent wind velocity vector v_a discussed in the next section.

[4]For further exposition on the differences between these operating states, see e.g., Prouty (pp. 94).

The velocity of the air is defined as a single vector called the "apparent wind velocity" denoted as v_a. This is the wind velocity relative to the quadcopter at any instant in time. In this simulation, this vector is the sum of 3 sources:

1. The motion of the quadcopter itself. In a completely still atmosphere, the quadcopter will see an apparent wind equal to the negative of its own velocity.
2. A "laminar" wind component. This component is the same at all points in the simulation domain.
3. A turbulent wind component. This is a small spatially varying perturbation, the source and simulation of which is discussed below.

The ambient temperature, relative humidity, and ambient pressure are constant throughout the simulation domain. These constants are used to calculate the ambient air density used, for example, in Equations 1-3. These parameters are also inputs to the auralization process (i.e., to calculate the speed of sound and atmospheric absorption).

Body Drag

The next effect comes in the form of a simple resistive drag term. This drag arises from any body moving through a gas, and always opposes the apparent wind velocity. In aircraft, it is known as 'parasitic' or 'body' drag, as it does not take into account drag generated by the components of the aircraft that create lift (in this case, the rotor surfaces).

The simplest implementation of this force comes in the form of the common drag equation (see, e.g., Bangura):

$$F_{d;Body} = \frac{1}{2}\rho v_a^2 C_D A \tag{13}$$

where ρ is the density of the air that the quadcopter is moving through, v_a is the magnitude of the apparent wind velocity from the previous section ($v_a = kv_a k_2$), C_D is the drag coefficient, and A is the projected surface area of the quadcopter.

For this basic model, the quadcopter is treated as the rectangular volume that encloses all of the components of the vehicle except for the rotors (that is, the motors are included at the extremity of the volume, but not the rotors themselves). Computing the projection of the quadcopter volume (modified by the quadcopter's current attitude) onto the 2-dimensional plane orthogonal to the direction of v_a will produce the area A in Equation 13.

The value of C_D is set to be .9, which is a typical value used for the drag coefficient of a cube with arbitrary orientation relative to the wind. This selection of C_D corroborates with work by Cano (Ref. 16).

The force generated by this drag acts at the center of the 'hub' of the quadcopter (see the Quad-Sim documentation for the explanation of the mass distribution). In the event that this 'aerodynamic center' is different from the center of mass, a torquing moment may be generated by this force.

Although this model is quite rudimentary, it is likely sufficient since drag created by the lifting surfaces (rotors) are the more significant factor, as discussed below.

Rotor Drag

There are at least 3 sources of drag forces that can act on the rotors of a quadcopter. The sum of these forces is known as the "H-force" in rotorcraft literature. Much of the development of this section comes from a synthesis of expressions that can be found throughout Prouty (Ref. 13). These results come from simplifications of blade element momentum theory.

Flapping Drag:

In forward flight, a spinning rotor will generate more thrust over the advancing side of the rotor disk than over the retreating side. This imbalance can lead to vehicle instabilities. To compensate for this effect, rotor blades are made to be somewhat flexible so that they bend as they spin, evening out the thrust. This flapping makes the entire rotor disk rotate backwards, creating a drag-like force opposite the direction of motion. The backwards force is proportional to both velocity and to rotor thrust.[5]

To calculate flapping drag, the collective pitch must first be determined as:

$$q_0 = \frac{\frac{4C_T}{\sigma a}\left[1+\frac{3}{2}\mu^2\right] - \frac{q_1}{2}\left[1-\frac{3}{2}\mu^2+\frac{3}{2}\mu^4\right]\left[\lambda^0 - 1 - \frac{\mu^2}{2}\right]}{\frac{2}{3}-\frac{2}{3}\mu^2+\frac{3}{2}\mu^4} \tag{14}$$

This equation has several components:

- a is the slope of the lift curve per radian. A value of 6.0 can be used for most rotors (Prouty, pp. 12).
- C_T is the nondimensional thrust coefficient defined earlier (Eq. 1).
- σ is the rotor solidity, which is the ratio of blade area to rotor disk area.
- q_1 is the blade twist from center to end, which is typically around -10 degrees (Prouty, pp. 13).
- μ is the tip speed ratio, which is the magnitude of the component of the apparent wind velocity v_a that is in the tip path plane divided by the tip speed v_t.
- λ^0 is the inflow ratio: the ratio of airflow through the rotor disk divided by tip speed (Prouty, pp. 166). It can be calculated as:

[5] Quadcopter blades are relatively stiff, so this effect is proportionally smaller — however still significant — than it would be for full-scale helicopters.

$$\lambda_0 = \frac{-(v_\bullet \sin\alpha + v_i)}{v_t} \tag{15}$$

Here $v_\bullet$, v_i, and α are defined as they were in Equation 8. The tip speed, given rpm w and rotor radius r, can be calculated simply as:

$$v_t = wr\frac{2\pi}{60} \tag{16}$$

Using these elements, the angle at which the rotor disk rotates against the direction of motion is (from Prouty, pp. 169):

$$a_{1;s} = \frac{m}{1-\frac{\mu^2}{2}}\left[\frac{8}{3}\theta_0 + 2\theta_1 + 2\mu\lambda_0 - \alpha\frac{v_i}{v_t}\right] \tag{17}$$

The force due to flapping drag (for a single rotor producing thrust T) is given as:

$$F_F = T\sin a_{1;s} \tag{18}$$

These forces act on the location of the center of each rotor. As with the body drag, since these forces are not acting on the center of mass, they will produce torquing moments on the quadcopter that must be taken into account.

Induced and Profile Drag:

In addition to drag from blade flapping, there are other components of rotor drag due to induced drag and profile drag. The coefficients for these remaining components of the H-force are given in Equation 19 (on page 7). In that equation c_d is the drag coefficient of the rotor, which can be assumed to be 0.01 for the entire operating envelope of the quadcopter (see the figure in Prouty, pp. 23). C_H can be used as a drag coefficient in order to find the force opposing the direction of motion:

$$F_{l;P} = C_H \rho A_r v_t^2 \tag{20}$$

where A_r is the projection of the rotor area and not the projected area of the quadcopter volume from the earlier body drag equation.

Turbulence

One of the starkest differences between Figures 1 and 2 is the lack of rapid fluctuation of the BPFs in the latter. In the real world, the free atmosphere is filled with small-scale turbulent eddies (including those that are about the size of a quadcopter). These eddies are likely the primary source of the fluctuations present in the recording. Accordingly, an effort was made to add a simple model for near-ground turbulence to the quadcopter model.

For this effect, the starting point is a model used for flight qualification for the US Military (Handbook #1797 (Ref. 17)). This model specifies how to generate a "velocity distance history," which is a data set that specifies the turbulent component of the apparent wind velocity at a given distance along a flight path[6]. This component is realized as velocities in the x, y, and z directions (positive-z being the direction away from the surface of the Earth). An example output for a 20 ft flight path is shown in Figure 3.

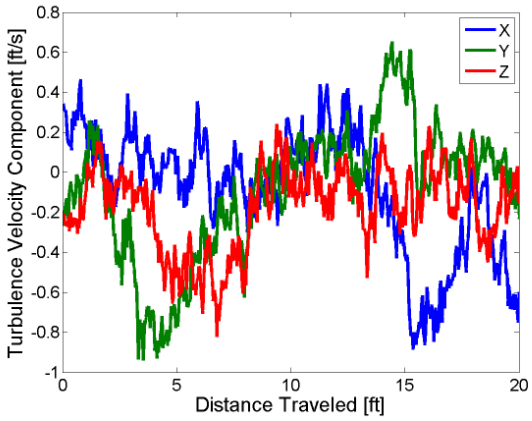

Fig. 3. An example velocity distance history.

There are a number of details needed to make this model compatible with the quadcopter simulation:

- The original specification gives different expressions for the eddy size distribution in the x and y directions (the directions of motion of the aircraft and that orthogonal to the direction of motion and the z direction, respectively). In quadcopter operations, the x and y directions are interchangeable, as a quadcopter is just as likely to fly in a circle as it is to go straight (whereas fixed-wing aircraft must fly primarily in a straight line in order to stay aloft). Accordingly, the expression for the x distribution of turbulent eddy length scales is made the same as that for the y distribution for this simulation.
- The specification also provides methods for computing the pitching, yawing, and rolling moments generated by the turbulent field on the aircraft. These expressions utilize the geometry of a fixed-wing aircraft (i.e., fuselage length and wingspan). For this application, these values are taken to be the distance between adjacent rotor centers.
- In the original specification, the eddy size distribution is given as a Dryden spectrum, whereas it is commonly understood that atmospheric turbulence is more closely rep-

[6]This nomenclature can be related to the term "pressure time history," which is common in acoustics, indicating a stream of data that is meant to describe how a measurement of pressure at a single point changes as time evolves.

$$\frac{C_H}{s} = \frac{c_d m}{4}\left(\frac{a}{4}\left(\frac{m\lambda'}{1+\frac{3}{2}m^2}\right)\left(q_0\left(\frac{1}{3}+\frac{3}{2}m^2\right)+\frac{q_1}{2}\left(1+\frac{3}{2}m^2\right)\lambda'\right)\right.$$
$$\left. + \frac{a}{4}\left(\frac{m}{1+\frac{1}{2}m^2}\right)\left(\frac{a_0^2}{2}\left(\frac{1}{9}+\frac{m^2}{2}\right)+\frac{1}{3}ma_0\frac{v_i}{v_t}+\frac{1}{8}\frac{v_i^2}{v_t^2}\right)\right) \quad (19)$$

resented by a von Kármán spectrum. The use of the Dryden spectrum in legacy applications allowed for the generation of an IIR filter that could produce the needed velocity distance histories. This effort is not constrained to use such filters and can therefore employ the von Kármán spectrum directly.

For completeness, the equations specifying the turbulent eddy length scales that were used are:

$$L_x = L_y = \frac{h}{2(0.177 + 0.000823h)^{6/5}} \quad (21)$$

$$L_z = \frac{h}{2} \quad (22)$$

where h is the height of the quadcopter above the ground in feet. The turbulence 'intensities' are:

$$s_x = s_y = \frac{s_z}{(0.177 + 0.000823h)^{2/5}} \quad (23)$$

$$s_z = 0.1W_h \quad (24)$$

where W_h is the wind speed at the specified height in ft/s. Lastly, the formula to generate a von Kármán power density function for any direction (x, y, z) and spatial frequency w is:

$$F_i(w) = s_i^2\frac{2L_i}{p}\frac{1+\frac{8}{3}(2.678L_i w)^2}{(1+(2.678L_i w)^2)^{11/6}} \quad (25)$$

These equations are valid (for this model) between 10 and 1000 ft. An IFFT can be used to produce the desired distance velocity histories as in Fig. 3 from the results of Eq. 25. Expressions for computing the pitching, yawing, and rolling moments from the above results are available in the original reference.

Deficiencies:

There are a number of immediate deficiencies that come with using this turbulence model in this application. Most arise from the fact that this model makes the assumption that the aircraft under study is traveling at a speed much greater than the speed of the turbulent eddies – both the speed at which the gas is moving within the eddy and the speed at which an eddy is evolving or translating through the atmosphere. This allows the use of a "frozen atmosphere" condition and the generation of the single distance time history as shown above.

In the case of sUAS vehicles, the speed of the aircraft is low enough that it may be commensurate to the advection velocities present in the a real turbulent field. Additionally, one of the main operational modes of many sUAS vehicles is hover — where the aircraft is (nominally) not moving at all. In this condition, the lack of motion of the vehicle would imply that the turbulence history is not advancing so that, in the extreme case, the vehicle equilibrates with a particular moment in the turbulence history (e.g., a zero-velocity crossing) and the effect of turbulence completely disappears.

There are several naïve methods of addressing this problem including forcing the distance velocity history to advance with the laminar wind speed or with the speed indicated by the current position in the turbulent velocity time history. As both of these ideas do not necessarily arise from the physics behind the model, and given that the model is an accepted standardized formulation, no attempt was made to include such modifications.

Manufacturing Error

In the recording shown in Figure 1, as well as in other recordings, it has been observed that the four rotor BPFs of quadcopters do not vary around the same nominal values. This is an expected effect, as one of the tasks during the setup of a quadcopter is to 'calibrate' a zero-point between the four rotors — where the forces being exerted are relatively balanced. This gives the PID control scheme a solid starting point and allows for important components of flight such as a smooth initial take-off.

These offsets in rpm translate to differences in mean frequencies for the blade passage harmonics in the sound generated by the quadcopter. When two sinusoids are sufficiently close to one another in frequency, human listeners will hear a "beating" effect instead of two distinct tones. In the recording, the mean frequencies are far enough apart that this effect is not heard. If these frequencies were closer or overlapping, one would hear an additional layer of interference effects between rotors that is absent in the recording of Fig. 1. This lack of beating is clearly a salient subjective feature of the recordings — as will be demonstrated below when observing the differences between auralizations that are generated with and without these "error" offsets.

In order to simulate this behavior, an optional random error term was built into the simulation. This error term applies a random (normally distributed) component to the torque coefficient C_T (from Equation 1 above) of the four individual rotors

of the quadcopter. This forces the PID control scheme to compensate for differences between rotors by changing their expected nominal operating BPFs. (For the simulator described here, unlike the real vehicle, the PID controller does this automatically and there is no need to pre-calibrate the system.)

AURALIZATION RESULTS

This section discusses the effects that arise from incrementally adding the simulation extensions discussed above. Without any of the extensions, the auralization spectrogram from the introduction is produced (Figure 2). That figure, as well as those shown below are all based on a simulation that attempts to recreate the flyover from the recording shown in Fig. 1. The baseline details of the simulations are mostly nominal values meant to reflect those either recorded during the flyover or intended by the operator. Also, the atmospheric parameters are chosen to approximate the conditions present on the recording day. These parameters are summarized in Table 1.

Table 1. Simulation/auralization parameters.

Parameter	Value	Unit
Altitude	18	ft
Speed	20	ft/s
Mass Distribution	DJI Phantom II	
Rotor Spec.	DJI Phantom II (OEM)	
Payload[a]	1	kg
Atmospheric Properties		
Temperature	20	°C
Pressure	101,325	Pa
Relative Humidity	50	%
Wind Speed[b]	12	ft/s
Auralization Properties		
Listener Location	h0; 0; 4i	ft
Ground Impedance	Rigid	

[a]Payload is symmetrically under-hung. The real payload was likely non-symmetric and closer to .6 kg.

[b]Wind direction is in opposition to the quadcopter direction of motion. Wind does not affect auralization processing.

Body Drag

The first introduced effect is the drag created by the body of the quadcopter passing through the air.[7] This drag is dependent on the apparent wind velocity — the velocity of the laminar wind component as well as the negative of the instantaneous velocity of the vehicle.

The addition of this effect serves to separate the BPFs of the front and rear motor pairs slightly, though not as much as is observed in the recording. In this simulation, the split is caused by two sources of torque balancing each other: One is the torque needed for the quadcopter to pitch forward in order to overcome the forward momentum that is lost to the drag on the body. The other is the moment created by gravity on the under-hung payload and components of the quadcopter (for the Phantom II, the center of mass, even without a payload, is below the rotor plane). If the total center of mass of the quadcopter and its payload was in plane with the rotors, this BPF-splitting effect would disappear.

[7]N.B. The upgrades discussed in the "Rotorcraft Aeromechanics" section above are included for all simulations.

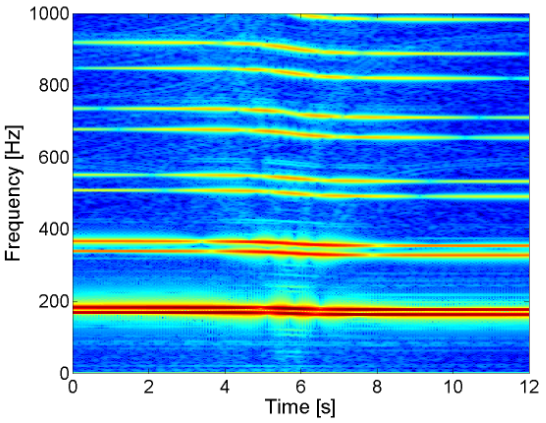

Fig. 4. Spectrogram of auralization: Only body drag included in the simulation. (All auralizations shown here use the basic model with the upgraded aeromechanics.)

Rotor Drag

Figure 5 shows the result of adding the sources of drag on the rotors to the simulation. This drag is added in accordance with the rotor geometry used and the assumptions noted in the development of this effect (above). In this case, the split between the front and rear motor BPFs is similar to that observed in the recording. There are two primary reasons why the rotor drag is much more effective at creating this split than the body drag:

1. The rotor drag creates a force on the vehicle that is directly related to the apparent wind velocity ($F_{d;rotor} \mu v_a$), whereas the drag caused by the body is proportional to the square of the apparent wind ($F_{d;body} \mu v_a^2$). The simulated vehicle is operating in the regime in which v_a is low enough that the rotor drag is dominant. If the vehicle were to be able to travel faster, it could get into the regime in which body drag became the dominant source of drag — where full-size rotorcraft and fixed-wing aircraft operate.

2. The addition of rotor drag creates a deleterious feedback effect on the operation of the vehicle. In order to maintain forward speed, the vehicle must tip forward so that some of the thrust of the rotors goes to replacing the forward momentum that is lost to drag effects (as with body drag). However, unlike body drag, the drag on an individual rotor is also proportional to the speed at which

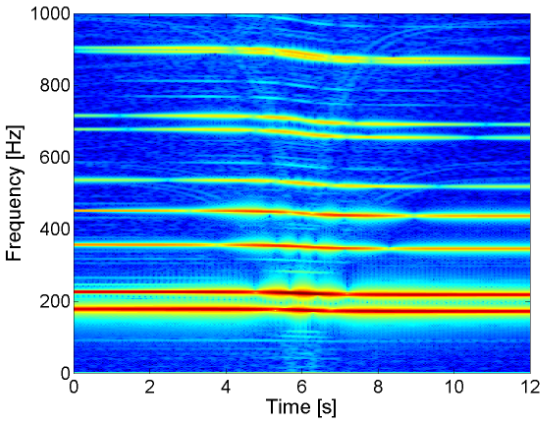

Fig. 5. Spectrogram of auralization: Body and rotor drag effects included in simulation.

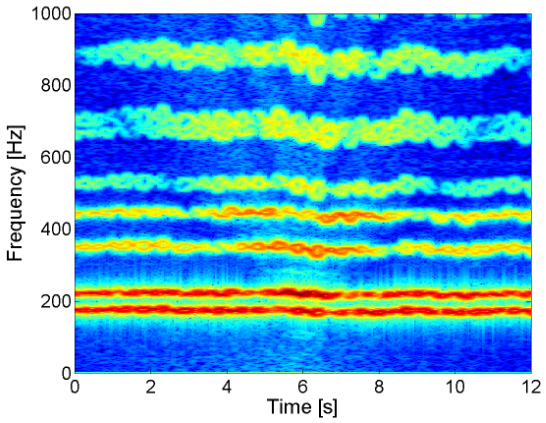

Fig. 6. Spectrogram of auralization: Drag effects and turbulence model included in simulation.

that rotor is spinning ($F_{d;rotor}$ µ rpm). Therefore, tipping forward creates a further differential drag between the front and rear rotor pairs — a force that acts to tip the vehicle back down (toward a neutral, 0-pitch, position). This feedback situation causes the large split in rpm that is observed.

For both of the reasons noted, but especially for the latter, rotor drag appears to be a critically important element to include in a quadcopter model meant for auralization. Also, as will be discussed next, it is an important effect to include in concert with simulations of turbulence.

Turbulence

Figure 6 shows the result of the addition of a turbulent component to the apparent wind field. It is important to note that the magnitude of this field is not an arbitrary choice and, in accordance with the turbulence model discussed above, is based on other parameters of the simulation including the height of the quadcopter above the ground and the laminar wind velocity.[8]

Comparing Figures 1 and 6, the depth of frequency modulation can be seen to be commensurate between the two sounds. That is, the BPF modulations induced by turbulence present at the site of the recording is on the order of those induced by the addition of the turbulence model to the simulation. There are longer variations that are present in the recording (e.g, the noticeable dip in BPF between 1 and 3 seconds in Fig. 1) that are not found in the simulation. This difference is likely due to the fact that the flyover that generated the recording was not a programmed 'way point' operation as is flown in the simulation, but was executed by a human pilot making adjustments in real time.

[8]The random seed that is used to generate the turbulent field is a controllable parameter of the simulation. Both Fig.s 6 and 7 (below) use the same random seed and therefore are impacted by the same turbulent velocity distance history.

One very important observation that is not evident from the figures is the fact that the turbulent field is affecting the vehicle primarily through rotor drag. Although not shown here, if the effect of rotor drag is turned off in the simulation, and turbulence is left on, the resulting auralization significantly lacks the BPF variation seen in the recording. This is again due to the fact that the turbulent components of v_a are quite small — on the order of 1 ft/s (see Fig. 3). Therefore, the component of drag that is proportional to v_a will have a much greater effect on the dynamics of the vehicle than the component that is related to v_a^2.

Manufacturing Error

The last effect to be added is the error term described above. The result of this simulation is shown in the spectrogram of Figure 7. Here, a normally distributed error of 10% — a typical manufacturing tolerance level for mass produced electronics — has been added to the nominal values of C_T for the 4 rotors. With this addition, the four traces of the BPFs do not overlap. This causes the interference effect present in the auralization of Fig. 6 to disappear. (Again, this effect is not observable in the spectrogram of Fig. 1, nor is it present when listening to the recording thereof.)

Another observed effect of this final case is the fact that the rear two motors are split in frequency by a smaller amount than the two front motors. This effect is not due to just the random draw of the errors added to C_T in this particular run, in fact this effect is seen in the vast majority of draws. The source of this effect comes from the fact that the thrust generated by an individual rotor is proportional to the square of the rpm of the rotor. Therefore, for rotors spinning more quickly (as the rear two are relative to the front two), a smaller adjustment needs to be made to their respective speeds to overcome the same magnitude of difference in C_T that may be present between the two due to this error term. It is interesting to note that not only was this effect not programmed into the

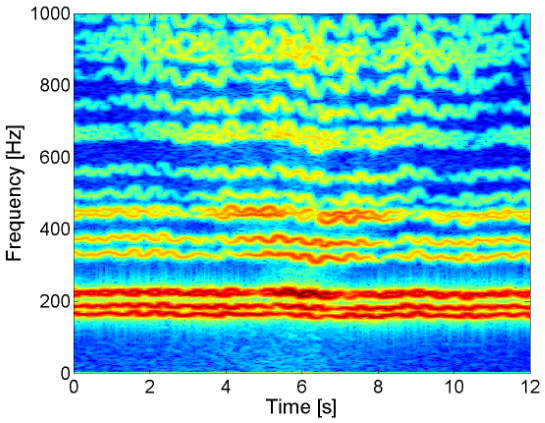

Fig. 7. Spectrogram of auralization: Drags, turbulence, and "error" included in simulation.

simulation explicitly, it was also not directly observed from the recording until after it was consistently observed in auralizations. In this way the developed tool chain of simulation and auralization wound up offering insights into the physics behind quadcopter flight that were emergent from the interactions of the programmed effects.

It is important to note that while the implementation of this error term has focused on direct manipulation of the value of C_T, there are some simple physical effects that could have caused this split in the recording:

- The presence of a non-centered payload. In the case of the recording, the payload was known to not have a center of mass directly underneath the physical center of the vehicle (although this offset was not measured).
- The presence of a laminar wind component that is not directly opposing the direction of movement of the vehicle. In general this will be the case in real-world conditions. Although the recording of Fig. 1 was taken when the quadcopter was flying into a stiff wind, it was not likely to have been perfectly aligned in opposition to the vehicle. The auralizations shown here are all based on simulations with a laminar wind that does perfectly oppose the (nominal) direction of motion of the vehicle.

CONCLUSIONS

This paper has outlined the current state of a quadcopter simulation capability that has been developed for the NASA DELIVER project. The development of the model from a number of sources was described. Incrementally adding effects to the simulation reveals how important each effect can be on an auralization based upon the model. Further, the ability to selectively turn on and off effects can provide insight into the source of aurally-significant details found in real-world data.

The principal result of this work so far (aside from the creation of the tool itself), is to point out the necessity of many of the effects included here if a simulation is to be used for auralization. For many other applications of quadcopter simulation (e.g., control scheme development), these effects are unnecessary and computationally expensive. However, the complicated and nuanced nature of the desired sound leads to a need for an equally complicated simulation capability.

Andrew Christian is the corresponding author. eMail: andrew.christian@nasa.gov

ACKNOWLEDGMENTS

Support for this work comes from the NASA DELIVER subproject. This is contained within the CAS project of the TAC program within the Aeronautics Research Mission Directorate.

Much of the technical work described here was produced during Joseph Lawrence's internship at NASA Langley during the summer of 2015. Accordingly, the facilitators and coordinators of the NIFS internship program deserve acknowledgment for providing the environment within which extraordinary steps are consistently taken by undergraduates in only 10 weeks. Eric Greenwood, Nik Zawodny, and other researchers in the Aeroacoustics Branch also deserve credit for their guidance on the rotorcraft aeromechanics section.

Lastly, a great deal of thanks is owed to Andrew's coworkers including: Kevin Shepherd, Stephen Rizzi, Ran Cabell, Menachem Rafaelof, Brian Tuttle, Aric Aumann and James Stephenson who have been infinitely helpful in accommodating his reduced capacity for work during a protracted (and ongoing) period of immoderate health.

REFERENCES

[1]Christian, A., Boyd, D. D., Zawodny, N. S. and Rizzi, S. A., "Auralization of tonal rotor noise components of a quadcopter flyover," Paper 209, InterNoise 2015, San Francisco, CA, August 9-12 2015.

[2]Rizzi, S. A., Sullivan, B. M. and Aumann, A. R., "Recent developments in aircraft flyover noise simulation at NASA Langley Research Center," NATO Research and Technology Agency AVT-158 "Environmental Noise Issues Associated with Gas Turbine Powered Military Vehicles" Specialists' Meeting, NATO RTA Applied Vehicle Technology Panel, Paper 17, Montreal, Canada, 2008.

[3]Rizzi, S. A. and Christian, A., "A method for simulation of rotocraft fly-in noise for human response studies," Paper 192, InterNoise 2015, San Francisco, CA, August 9-12 2015.

[4]Faller, K. J., Rizzi, S. A. and Aumann, A. R., "Acoustic Performance of a Real-Time Three-Dimensional Sound-Reproduction System," National Aeronautics and Space Administration NASA/TM-2013-218004, June 2013.

[5]Cabell, R., McSwain, R. and Grosveld, F. "Measured Noise from Small Unmanned Aerial Vehicles," NoiseCon 2016, Providence, RI, June 13-15, 2016.

[6]Palumbo, D., Rathsam, J., Christian, A. and Rafaelof, M., "Perceived annoyance to noise produced by a distributed electric propulsion high lift system ," AIAA Aviation Conference 2016, Washington D.C., June 13-17 2016.

[7]D. Hartman, K. Landis, M. Mehrer, S. Moreno and J. Kim, Quad-Sim, 2014.
¡https://github.com/dch33/Quad-Sim¿

[8]Mahony, R., Kumar, V. and Corke, P., "Multirotor Aerial Vehicles: Modeling, Estimation, and Control of Quadrotor," IEEE Robotics & Automation Magazine, No. 19, 20-32 2012.

[9]Bangura, M. and Mahony, R., "Nonlinear Dynamic Modeling for High Performance Control of a Quadrotor," Australasian Conference on Robotics and Automation, December 2012.

[10]Aumann, A. R., Tuttle, B. C., Chapin, Wm. L. and Rizzi, S. A., "The NASA Auralization Framework and plugin architecture," InterNoise 2015, San Francisco, CA, August 9-12 2015.

[11]Atkinson, K. and Han, W., Elementary Numerical Analysis (3rd Ed.), John Wiley & Sons, Hoboken, NJ, 2004.

[12]Hoffmann, G. M., Huang, H., Waslander, S. L. and Tomlin, C. J., "Quadrotor helicopter flight dynamics and control: Theory and experiment," Proc. of the AIAA Guidance, Navigation, and Control Conference. Vol. 2. 2007.

[13]Prouty, R. W., Helicopter Performance, Stability, and Control, Krieger Publishing Company, Inc., 1986.

[14]Leishman, J. G., Principles of Helicopter Aerodynamics, Cambridge University Press, New York, NY, 2000.

[15]Zawodny, N. S., Boyd, D. D., and Burley, C. L., "Acoustic Characterization and Prediction of Representative, Small-Scale Rotary-Wing Unmanned Aircraft System Components," American Helicopter Society 72nd Annual Forum, 2016.

[16]Cano, J. M., "Quadrotor UAV for wind profile characterization," Universidad Carlos III de Madrid, 2013.

[17]Department of Defense (U.S.) Handbook, "Flying Qualities of Piloted Aircraft," MIL-HDBK-1797, 19 December 1997.